Available online at www.sciencedirect.com
SCIENCE DIRECT
Biochimica et Biophysica Acta 1716 (2005) 29 – 39
BIOCHIMICA ET BIOPHYSICA ACTA
BBA
http://www.elsevier.com/locate/bba

Investigation of a novel artificial antimicrobial peptide by fluorescence correlation spectroscopy: An amphipathic cationic pattern is sufficient for selective binding to bacterial type membranes and antimicrobial activity

Lanlan Yu [a], Jeak Ling Ding [b], Bow Ho [c], Thorsten Wohland [a,*]

[a] *Department of Chemistry, National University of Singapore, 3 Science Drive 3, 117543, Singapore*
[b] *Department of Biological Sciences, National University of Singapore, 14 Science Drive 4, 117543, Singapore*
[c] *Department of Microbiology, National University of Singapore, 5 Science Drive 2, 117597, Singapore*

Received 9 May 2005; received in revised form 22 July 2005; accepted 17 August 2005
Available online 30 August 2005

Abstract

Fluorescence Correlation Spectroscopy (FCS) is used to study the interaction of a recently designed antimicrobial peptide, called V4, with LPS and lipids of varying head and tail groups. V4 is designed based on a known amphipathic cationic pattern BHPHB (B: basic; H: hydrophobic; P: polar residue, respectively) and shows a good combination of high antimicrobial activity, low cytotoxic activity and low hemolytic activity. It is shown that V4 has high binding affinity for LPS, which is the major component of the outer membrane of Gram-negative bacteria, and shows selectivity for negatively charged lipids in contrast to zwitterionic lipids at a low peptide/lipid ratio. At high peptide/lipid ratio, V4 can permeabilize vesicles composed of negatively charged lipids and eventually cause vesicle fusion. The identification of the amphipathic cationic pattern as the mediator of selectivity and antimicrobial activity could be a first step in the rational design of better antimicrobial peptides.

Keywords: Antimicrobial peptide; Fluorescence correlation spectroscopy

1. Introduction

Antibiotics are widely used for therapy of bacterial infection. However, extensive clinical use of antibiotics has caused an increase in antibiotic resistance, which makes it necessary to look for and develop new drugs [1–3]. Emerging potent candidates are antimicrobial peptides which are found in different organisms including insects, amphibians and mammals [4–7] and which play a major role in the host defense against microbial infection. Based on their structure, antimicrobial peptides can be divided into three main groups: α-helix, β-sheet and peptides rich in certain amino acid residues [8]. The α-helical conformation which is adopted by most linear antimicrobial peptides is usually induced when these peptides are in a hydrophobic environment such as a membrane, in lipid or detergent. The well-known insect cecropins [9] and frog magainins [4] belong to this group. Antimicrobial peptides with a β-sheet conformation usually possess disulfide bonds which are used to stabilize the conformation. Examples of this group include mammalian defensins [10,11] and protegrins [12,13]. The third group of antimicrobial peptides is mainly composed of certain specific amino acids. For example, the peptide tritrpticin [14] and indolicidin [15] are both rich in tryptophan and histatin is rich in histidine [16,17].

Antimicrobial peptides are thought to interact with lipopolysaccharides (LPS) which form a major part of the bacterial outer membrane in Gram-negative bacteria. LPS which is negatively charged is composed of three parts: O-antigen,

Abbreviations: V4, CVKVQVKVGSGVKVQVKVC; Rho 6G, Rhodamine 6G chloride; TMR, tetramethylrhodamine; R18, octadecyl rhodamine B chloride; LPS, lipo-polysaccharide; FITC-LPS, fluorescein isothiocyanate lipopolysaccharide; PBS, Phosphate buffered saline; PC, Phosphatidylcholine; DPPC, 1,2-Dipalmitoyl-*sn*-Glycero-3-Phosphocholine; DPPE, 1,2-Dipalmitoyl-*sn*-Glycero-3-Phosphoethanolamine; DPPG, 1,2-Dipalmitoyl-*sn*-Glycero-3-[Phospho-rac-(1-glycerol)]; POPC, 1-Palmitoyl-2-Oleoyl-sn-Glycero-3-Phosphocholine; POPE, 1-Palmitoyl-2-Oleoyl-*sn*-Glycero-3-Phospho-ethanolamine; POPG, 1-Palmitoyl-2-Oleoyl-*sn*-Glycero-3-[Phospho-rac-(1-glycerol)]; Rho-PE, 1,2-Dipalmitoyl-*sn*-Glycero-3-Phospho-ethanolamine-N-(Lissamine Rhodamine B Sulfonyl) (Ammonium Salt)

* Corresponding author.
E-mail address: chmwt@nus.edu.sg (T. Wohland).

0005-2736/$ - see front matter © 2005 Elsevier B.V. All rights reserved.
doi:10.1016/j.bbamem.2005.08.005

polysaccharide and lipid A. Lipid A is the conserved bioactive component of LPS which is responsible for most of the endotoxic effects. It has been shown that lipid A is the main interacting partner with antimicrobial peptides [18]. Using antimicrobial peptides to neutralize LPS, especially lipid A, is believed to be an effective approach to kill bacteria.

Although more than 800 antimicrobial peptides have been identified in eukaryotes (http://www.bbcm.units.it/~tossi/amsdb.html, Antimicrobial Sequences Database), these peptides are usually not fit for medical use due to their cytotoxic and hemolytic effects. There is therefore a need to design novel antimicrobial peptides with low cytotoxicity and low hemolytic activity. One strategy followed is the identification of the LPS binding domains on selected antimicrobial peptides and the design of new peptides containing these binding sites. Screening for high antibacterial activity, low cytotoxicity and low hemolytic activity can then be used for selection of potential drug candidates.

It has been well known that most natural antimicrobial peptides are net positively charged and also harbor some hydrophobic amino acid residues in spite of considerable variation in their primary structure and length [19]. Known peptide structures and computational models show an amphipathic cationic pattern BHPHB (B: basic; H: hydrophobic; P: polar residue, respectively) as a possible binding site of antimicrobial peptides to LPS [18]. Based on this pattern, a series of peptides have been designed and it was shown that amongst these, a peptide named V4 is prominent. V4 has a good combination of high antimicrobial activity, low cytotoxic activity and low hemolytic activity compared to other designed and natural peptides [20].

In the present work, we used fluorescence correlation spectroscopy (FCS) to investigate the interaction of this novel artificial peptide V4 with different membrane components. FCS is a technique that has been developed more than 30 years ago and relies on the measurement of fluorescence from a small, femtoliter size confocal volume [21]. A statistical analysis of the fluctuations in the fluorescence signal via an autocorrelation function yields information about the molecular processes underlying these fluctuations. The potential of FCS has been described in many recent reviews [22–26]. In biophysical applications in particular, FCS gives information, about concentration, binding, and aggregation of different components in a sample. In particular, FCS has been used to study the interaction of peptides with lipids [27,28]. In this study we use these capabilities of FCS to (i) obtain information about the oligomerization or aggregation state of V4, (ii) compare the affinity of binding of V4 for different lipid components of mammalian and microbial membranes and (iii) examine the influence of V4 on the integrity of lipid bilayers of different composition. From the data, we have gained insights into the possible mechanisms of action of V4 and can obtain suggestions on how to improve on the design of artificial antimicrobial peptides.

2. Materials and methods

2.1. Materials

Rhodamine 6G chloride (Rho 6G), tetramethylrhodamine (TMR) and octadecyl rhodamine B chloride (R18) are products from Molecular Probes (ITS Science and Medical Pte Ltd., Singapore). Lipopolysaccharide from *Escherichia coli* strain 0111:B4 (LPS), its fluorescent derivative fluorescein isothiocyanate lipopolysaccharide (FITC-LPS), Lipid A from *Escherichia coli* strain F583, Triton-X100 and Phosphate buffered saline (PBS) were purchased from Sigma-Aldrich (Sigma-Aldrich Pte Ltd., Singapore). DMSO was purchased from Mallinckrodt Baker (Mallinckrodt Asia Pacific Pte. Ltd., Singapore). Phosphatidylcholine (PC), 1,2-Dipalmitoyl-*sn*-Glycero-3-Phosphocholine (DPPC), 1,2-Dipalmitoyl-*sn*-Glycero-3-Phosphoethanolamine (DPPE), 1,2-Dipalmitoyl-*sn*-Glycero-3-[Phospho-rac-(1-glycerol)] (DPPG), 1-Palmitoyl-2-Oleoyl-*sn*-Glycero-3-Phosphocholine (POPC), 1-Palmitoyl-2-Oleoyl-*sn*-Glycero-3-Phosphoethanolamine (POPE) and 1-Palmitoyl-2-Oleoyl-*sn*-Glycero-3-[Phospho-rac-(1-glycerol)] (POPG), 1,2-Dipalmitoyl-*sn*-Glycero-3-Phospho-ethanolamine-N-(Lissamine Rhodamine B Sulfonyl) (Ammonium Salt) (Rho-PE) were purchased from Avanti (Avanti Polar Lipids, Inc., Alabaster, AL).

2.2. Peptides

The sequence of V4 is CVKVQVKVGSGVKVQVKVC with cyclization by a disulfide bond at the two terminal cysteines (C). Four lysine (K) residues provide high net positive charge and eight valine (V) residues make this peptide highly hydrophobic. V4-TMR is the V4 labeled with TMR at the N-terminus. Both peptides were synthesized by Genemed (Genemed Synthesis, Inc., South San Francisco, CA). According to the HPLC data provided by the company, the purity of V4-TMR is about 84% and the purity of V4 is above 97%. The stock solution of V4-TMR peptide was prepared as a 2-mM solution in DMSO. The stock solution of V4 was prepared as 1 mM in water. Both stock solutions were stored at −20 °C in small aliquots until further use.

2.3. Small unilamellar vesicles (SUVs) preparation

All lipids were prepared as stock solutions in chloroform or a mixture of chloroform and ethanol (4:1). The solvent was evaporated under N_2 gas and then the samples were placed into vacuum for at least 1 h. PBS buffer, pH 7.4, was added to re-dissolve the lipids to give an aqueous suspension of phospholipids at a concentration of 0.5 mM. SUVs were prepared by freeze–thawing the lipid suspension 5 times followed by extrusion through 0.05 μm polycarbonate membrane filters 20 times using a mini-extruder syringe device (Avanti Polar Lipids). The extruded lipid solutions were diluted and mixed with 200 nM V4-TMR to study the interaction of peptide and lipid vesicles by FCS.

2.4. Fluorophore entrapped vesicle preparation

The preparation followed a similar protocol as for LUVs. After removing the solvent from the lipids, PBS including Rho 6G was added to prepare suspensions of phospholipids. After 5 freeze–thaw cycles the suspension was extruded through 0.1 μm membranes. MicroSpin™ S-200 HR Columns (Amersham Biosciences, Singapore) were used to remove non-entrapped Rho 6G from the vesicle solution [27].

2.5. Fluorophore labeled vesicle preparation

Confocal imaging was taken with LUVs which were labeled with 1% Rho-PE. Fluorophore labeled vesicles were prepared by mixing POPG with a content of 1% Rho-PE in chloroform. After removing the solvent completely, PBS was added to make a suspension of phospholipids. The fluorophore labeled LUVs were obtained by freeze–thawing lipid suspension 5 times followed by extrusion 20 times through 0.1 μm polycarbonate membrane filters.

2.6. Fluorescence correlation spectroscopy (FCS)

FCS is a biophysical technique with single molecule sensitivity. It analyzes fluorescence intensity fluctuations caused by minute deviations from thermal equilibrium from a confocal volume in a sample which contains fluorescent particles [21,24,29,30]. For 3D diffusion processes, including a possible triplet

state of the fluorophores, the measured fluorescence photon count rates autocorrelation function (ACF) can be fitted by

$$G(\tau)=\frac{\gamma}{N}\frac{\sum_{i=1}^{n}\left(\frac{Q_i}{Q_1}\right)^2 F_i g_i(\tau)}{\left[\sum_{j=1}^{n}\frac{Q_i}{Q_1}F_i\right]^2}+G_\infty \tag{1}$$

with

$$g_i(\tau)=\left(1+\frac{\tau}{\tau_{Di}}\right)^{-1}\left(1+\frac{\tau}{\left(\frac{z}{\omega}\right)^2\tau_{Di}}\right)^{-1/2}\left(\frac{T_i e^{-\tau/\tau_{Ti}}}{1-T_i}+1\right) \tag{2}$$

and the diffusion time of species i

$$\tau_{Di}=\frac{\omega^2}{4D_i} \tag{3}$$

N is the average number of particles in the confocal volume and γ is a correction factor for the photon count rates distribution in the confocal volume [22,31–33]. The factor γ is a constant correction factor and we neglect it in further equations. To recover absolute concentrations we calibrated the system with a 1-nM fluorophore solution and set all other values in relation to this calibration. The fluorescence yields Q_i are the product of the extinction coefficient, the quantum yield, and the overall detection efficiency for particle i in the instrument. The coefficients F_i are the mole fraction of species i in the sample and g_i (τ) is the characteristic function of the underlying process that causes the fluctuations. T_i is the average fraction of particles of species i that reside in the triplet state and τ_{Ti} is the relaxation time due to the transition of the dye between the ground state and the first excited singlet and triplet state [40]. τ_{Di} is the lateral diffusion time of the fluorescent particle staying in the confocal volume. D_i is the diffusion coefficient of species i, and ω and z are the radial and axial distances of the confocal volume at which the photon count rates has dropped by $1/e^2$ of the maximum value. G_∞ is the convergence value of the ACF for long times, in general this value is 1. The program IgorPro (Wavemetrics, Lake Oswego, OR, USA) was used for fitting of the autocorrelation function to experimental data as described previously [34].

The fluorescence yields Q_i are important parameters in FCS. They determine the signal to noise ratio [35] but are as well a characteristic value for a fluorophore in a certain environment. Therefore, determining the value of Q of a particle can yield information which can help identify a fluorophore and can give information about the local environment of the fluorophore. For a solution with a single fluorophore present and negligible background it is simply given by the number of average photon count rates, C_1, divided by the average number of particles in the confocal volume, N_1 as obtained from the ACF.

$$Q_1=\frac{C_1}{N_1} \tag{4}$$

In solutions with two different fluorophores and photon count rates C_{12}, the autocorrelation amplitude which is inversely proportional to the apparent number of particles N_{app} is given by (Eq. (1) with $i=2$):

$$\begin{aligned}G(0)-G_\infty=\frac{1}{N_{\mathrm{app}}}&=\frac{1}{N}\times\frac{F_1+\left(\frac{Q_2}{Q_1}\right)^2F_2}{\left(F_1+\left(\frac{Q_2}{Q_1}\right)F_2\right)^2}\\&=\frac{1}{N}\frac{(1-F_2)+\left(\frac{Q_2}{Q_1}\right)^2F_g}{(1-F_2)+\left(\frac{Q_2}{Q_1}F_2\right)^2}\end{aligned} \tag{5}$$

$$C_{12}=N_1Q_1+N_2Q_2 \tag{6}$$

In this case, the values of Q can in general not be unambiguously determined if the concentration of the second species is not known. However, in the case that the number of particles N_1 and the fluorescence yield Q_1 for one of the fluorophores is known, e.g. if a fluorescent species of constant concentration is present in the samples, then F_2 (note that $F_2=1-F_1$) and Q_2/Q_1 can be calculated from Eqs. (4)–(6):

$$\frac{Q_2}{Q_1}=\left(\frac{N_1}{N_{\mathrm{app}}}\left(\frac{C_{12}}{C_1}\right)^2-1\right)\left(\frac{C_{12}-C_1}{C_1}\right)^{-1} \tag{7}$$

$$F_2=\left(1+\frac{N_1}{N_{\mathrm{app}}}\left(\frac{C_{12}}{C_{12}-C_1}\right)^2-\left(\frac{C_1}{C_{12}-C_1}\right)^2\right)^{-1} \tag{8}$$

The values thus obtained can then be used to identify the second particle or make predictions of its environment. This method was used to calculate the fluorescence yield and concentration of lipid-bound V4-TMR in the presence of a constant fluorescent impurity with known fluorescence yield, assumed to be free TMR.

In this work, all values have been corrected for background photon count rates [35,36] and refer to the uncorrected values for the number of particles as N_{meas} and to the corrected values as N_{c}. B is the photon count rates of background which in this work is referred to the photon count rates of PBS solution. The number of particles is corrected by the Eq. (9).

$$N_{\mathrm{c}}=N_{\mathrm{meas}}\times\frac{\langle F\rangle}{\langle F+B\rangle^2} \tag{9}$$

If one fluorescent species is present, N_{c} is N. If two fluorescent species are present, then N_{meas} is used to describe the inverse of the amplitude, N_{app} is the background corrected value N_{c} (Eq. (5)), N is the number of particles corrected for background and different fluorescence yields, and F_2 describes the mole fraction of the second species.

2.7. FCS instrumentation

FCS experiments were performed using an Axiovert 200 inverted microscope (Carl Zeiss South East Asia, Singapore). The laser was focused on the samples using a water immersion objective (C-Apochromat, 63×, NA 1.2, Zeiss). A dichroic filter (560DRLP, Omega, microLAMBDA Pte Ltd., Singapore) and an emitter (595AF60, Omega) were used to separate the excitation light from the emission fluorescence. The samples were excited with the 530-nm line of laser beam from an Argon-Krypton laser (Melles Griot SP, Pte Ltd., Singapore). A 50 μm diameter pinhole (Wilson Engineering (S) Pte Ltd., Singapore) in the image plane blocked out-of-focus signals. The emitted fluorescence was detected by an avalanche photo diode (PerkinElmer Canada Inc., Canada) detector and then the signals were sent to a digital correlator (Model: Flex02-12D, http://www.correlator.com) to be autocorrelated.

2.8. Interaction of V4 with R18

200 nM unlabeled V4 was titrated by 10 nM R18 in PBS buffer. FCS experiments were performed at room temperature.

2.9. Interaction of V4-TMR with LPS

The stock solution of V4-TMR in DMSO (2 mM) was diluted with PBS to 100 nM. LPS was dissolved in PBS to different concentrations (50, 100, 150, 200, 300, 400, 500, 600, 700, 1000, 2000 and 10,000 nM). The mixture of peptide and different concentrations of LPS were incubated for at least 4 h to reach equilibrium. FCS experiments were performed at room temperature.

2.10. Interaction of V4 with FITC-LPS

500 nM FITC-LPS and different concentrations of V4 (10 nM, 100 nM, 1 μM) were mixed followed by at least 4 h incubation. FCS measurements were performed using the 488 nm Argon-Krypton laser line for excitation at a power

of 10 μW. The emission light was filtered by a dichroic filter (505DRLP) and a bandpass filter (530DF30).

2.11. Interaction of V4-TMR with lipid A and PC

Lipid A and PC were dissolved in PBS respectively and diluted to 10 μM. The mixture of V4-TMR and lipid A or PC was incubated for at least 4 h for FCS experiments.

2.12. Interaction of V4-TMR with SUVs

The procedure is similar to that of interaction of V4-TMR with LPS. The SUVs solutions with different lipid compositions were diluted to 50 μM (lipid concentration) and incubated with 200 nM V4-TMR for at least 4 h followed by FCS experiments.

2.13. Interaction of V4 with fluorophore entrapped LUVs

The stock solution of fluorophore entrapped LUVs was diluted to 20 μM (lipid concentration). 10 μM V4 was added into the above solution. The FCS experiments were performed by mixing the peptide and LUVs solutions in situ.

2.14. Fluorescence confocal imaging

Studies of V4-TMR attachment on glass coverslips and of the effect of V4 on fluorophore labeled LUVs were performed with a confocal microscope (FluoView™ FV300, Olympus, Singapore), equipped with a HeNe laser (543 nm) for excitation, a water-immersion objective (UPlanApo, 60×, NA1.2, Olympus) and a long pass emission filter at 560 nm. In the study of attachment of V4-TMR on glass coverslips (0.17 mm thick, Fisher Scientific Pte Ltd., Singapore), a PBS solution with either 100 nM TMR, 5 μM V4-TMR or 5 μM V4-TMR with 50 μM LPS were placed on the coverslilp and a stack of 60 confocal images of each solution were acquired from 15 μm below coverslip to 45 μm above coverslip with a step size of 1 μm. The average fluorescence intensity of each confocal image was calculated and the values for the surface and solution were reported.

For the study of the action of V4 on fluorescently labeled LUVs, the stock solution of 1% fluorescently labeled LUVs was diluted to 20 μM (lipid concentration) and placed on a coverslip. A stack of 20 confocal images was acquired from bottom to top with a step size of 1 μm. After addition of 10 μM V4 the same procedure was followed.

3. Results

3.1. Calibration of the FCS setup

The FCS setup was first calibrated with a 1-nM solution of TMR in PBS. Measurements were performed in 6 replicates and fitted with a one-particle model. The laser power was set to 100 μW before entering the microscope. The background photon count rates of PBS buffer were 0.9 kHz. The average number of particles measured was $N_{meas}=0.388\pm0.006$ and the average diffusion times was $\tau_D=56.9\pm0.8$ μs. After background correction the number of particle was $N=0.349$ and fluorescence yield Q was calculated to be 51.6 kHz (Eq. (4)). The structure factor was $K=4.6\pm0.4$, and the convergence value for long correlation times was $G_\infty=1.000\pm0.001$. In all other measurements K was fixed and G_∞ was always close to 1 and will not be further discussed in this work. The diffusion time of micellar LPS was identified to be 1.77 ± 0.50 ms by using FITC-LPS. The diffusion time of lipid SUVs was determined to be in the range of 1.3 to 3.5 ms by labeling with the amphipathic dye R18.

3.2. Solubility of V4-TMR

First the solubility was tested in PBS buffer. For V4-TMR solutions of 1 nM the photon count rates were at background level and no correlations could be detected. We have subsequently chosen concentrations of 100–200 nM of V4-TMR for FCS measurements. At a concentration of 100 nM the average number of particles measured was $N_{meas}=0.098\pm0.004$. There was one species in the solution with $\tau_D=52.5\pm1.8$ μs. After background correction the number of particle was $N=0.064$ and Q was determined to be 59.5 kHz. Because of the similar τ_D and Q of V4-TMR and of free TMR, it is likely that the measured particles correspond to free TMR and represent an impurity. Only on rare occasions some strong peaks could be observed in the photon count traces. A two-particle model had to be used in those cases where the second particle had a fraction usually smaller than 10% and a strongly variable τ_D of 684 ± 440 μs. These peaks might point towards peptide aggregation.

To test for peptide aggregation in PBS, unlabeled V4 solutions were titrated with the amphipathic dye R18. In these experiments, large aggregates were detected as shown by the large τ_Ds and distinct peaks in the photon count traces (Fig. 1). The diffusion time distribution of aggregates was quite wide, ranging from several hundreds of microseconds to tens of milliseconds. These experiments indicate that V4-TMR is aggregated and the fluorescence is strongly quenched. Therefore we tried to dissolve V4-TMR in different solvents. Due to the hydrophobic and positively charged characteristic of V4, we tried DMSO as well as the

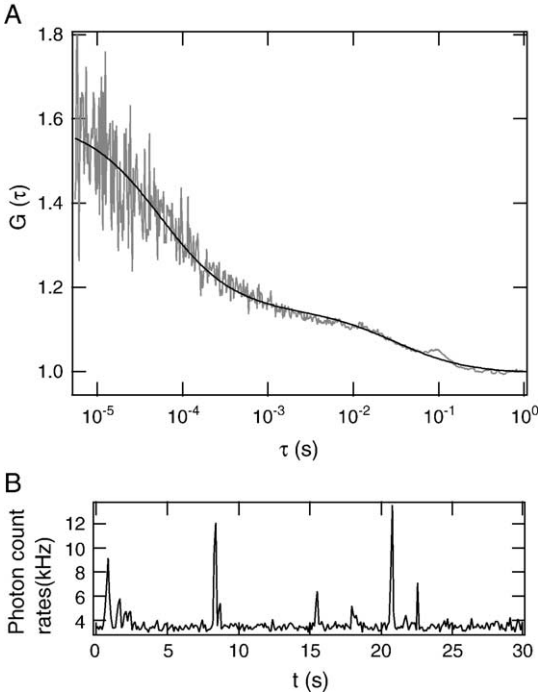

Fig. 1. The amphipathic dye R18 incorporates into V4 aggregates. (A) Autocorrelation function of 200 nM unlabeled V4 in presence of 10 nM R18. The solid line is the fit to the data depicted in grey. $N_{meas}=1.669$; $\tau_{D1}=54.4$ μs; $\tau_{D2}=31.0$ ms. (B) Photon count rates trace of V4 with R18.

detergent Triton-X100 to overcome the hydrophobicity, and alternatively pure de-ionized water to minimize ions that could shield the positive charges and facilitate aggregation (Fig. 2).

In PBS, 200 nM V4-TMR yielded an N_{meas} of 0.182±0.008. In Triton-X100, at the same V4-TMR concentration N_{meas} was 5.167±0.737, which is an increase of a factor 28. A two-particle model was used to fit the data and besides a fast species with 53.7±1.0 μs, which is assumed to be free TMR, a slow species was detected with τ_D=317±47 μs.

In de-ionized water N_{meas} was 0.635±0.076 which is an increase of a factor 3.5 compared to PBS solutions. In this case, V4-TMR solutions also showed two τ_Ds, one again similar to free TMR and the other 447±30 μs.

In DMSO strong quenching was observed and the measured number (compared to a calibration with 1 nM Rho 6G in DMSO) rose by a factor 2.1. Although an increase in N_{meas} can be observed in the different solvents, the value of N_{meas} always remained below the expected value by almost a factor 20 in the best case (Triton-X100). This is also supported by NMR measurement of V4-TMR which showed broadened peaks indicating peptide aggregation (data not shown). In the rest of the work, experiments have been performed in PBS solution since it is physiologically the most relevant condition.

3.3. Binding of V4-TMR to LPS

The putative target molecule for antimicrobial peptides in the outer membrane of bacteria is LPS [37]. Therefore, at a concentration of 100 nM V4-TMR, increasing concentrations of LPS were added to test for binding activity. The dependence of the ACF on the concentration of LPS is shown in Fig. 3. Two components can be distinguished in solution, a fast diffusing species (fixed at τ_{D1}=52 μs) and an average slow diffusing species (τ_{D2}=1.36±0.17 ms) with a diffusion time similar to that of LPS micelles (τ_D=1.77±0.50 ms). With

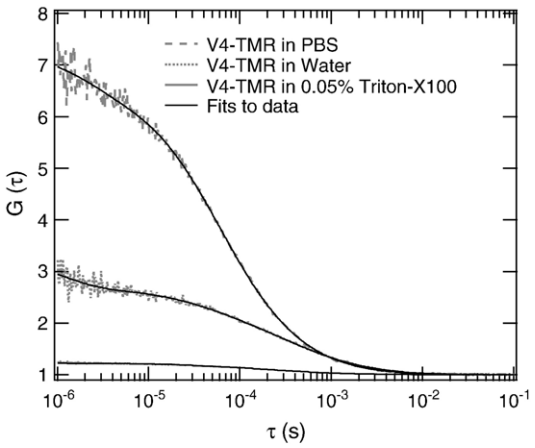

Fig. 2. Autocorrelation function of 200 nM V4-TMR in PBS, water and 0.05% Triton-X100. The measured particle numbers are as follows: $N_{V4\text{-}TMRPBS}$=0.182±0.008, τ_{D1}=56.7±0.5 μs, τ_{D2}=684±440 μs; $N_{V4\text{-}TMRwater}$=0.635±0.076, τ_{D1}=54 μs (fixed), τ_{D2}=447±30 μs; $N_{V4\text{-}TMRTriton\text{-}X100}$=5.167±0.737, τ_{D1}=54 μs (fixed), τ_{D2}=317±47 μs.

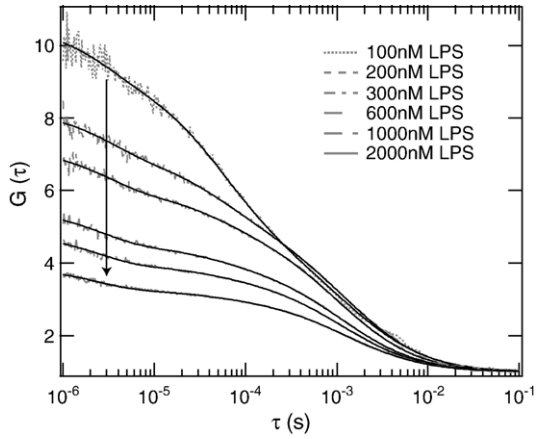

Fig. 3. Autocorrelation functions of 100 nM V4-TMR with different concentrations of LPS in PBS. With increasing concentrations of LPS (100–2000 nM), the amplitude of the autocorrelation function decreased as indicated by the arrow and a longer diffusion time (τ_{D2}=1.36±0.17 ms) with a constantly increasing fraction appeared (for the fraction see Fig. 4). Fits to the data are given as solid lines.

increasing concentrations of LPS, the amplitude of the ACF decreased continuously, indicating an increasing number of fluorescent particles in the confocal volume. At the same time, the overall photon count rates increased synchronously with the apparent number N_{app} (Fig. 4A). In controls of TMR/LPS mixtures, no change in amplitude or intensity could be observed.

Assuming that the fast diffusing species corresponds to a constant impurity of free TMR, the fluorescence yield Q_2 of the slower diffusing species can be obtained (Eq. (7)). N_{app} and C_{12} are obtained directly from measuring mixtures of V4-TMR and LPS after background correction. N_1 and C_1 are determined from V4-TMR solution assuming that only free TMR was detected and aggregates are mostly quenched. The V4-TMR: LPS complex is 1.73±0.28 times as bright as free TMR. The fluorescence yield Q_2 of V4-TMR: LPS is calculated to be 102.9 kHz. The fraction F_2 and number of V4-TMR: LPS complexes N_2 in the confocal volume are plotted in Fig. 4B and C in dependence on the LPS concentration (see Eq. (8)). Both, F_2 and N_2 rise with increasing LPS concentrations up to F_2=80% and N_2=0.27 at an LPS concentration of 2 μM after which these values stay constant.

3.4. Binding of unlabeled V4 to FITC-LPS

At a FITC-LPS concentration of 500 nM and unlabeled V4 concentrations between 10 nM and 1 μM, no change in τ_D or N were seen.

3.5. Attachment on the coverslip surface

Because of the hydrophobicity of V4-TMR, the effect of glass coverslips on V4-TMR was investigated by taking confocal images of the surface and the solution and calculating their respective average fluorescence intensities (Table 1).

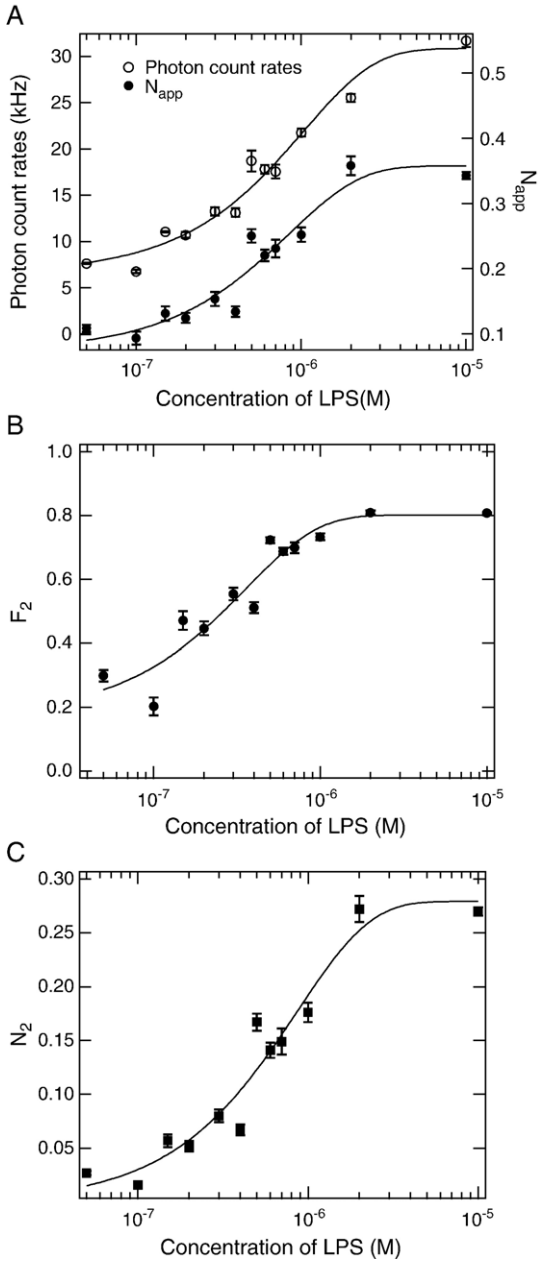

Fig. 4. Titration of 100 nM V4-TMR with increasing concentrations of LPS (50 nM–10 μM). (A) Photon count rates and apparent number of particles in the confocal volume in dependence on LPS concentrations. (B) The mole fraction F_2 in the solution increased with increasing concentrations of LPS and reached saturation around 80%. (C) The number of V4-TMR: LPS complexes N_2 in the confocal volume increased with the increasing concentrations of LPS. Solid lines are added to guide the eye.

3.6. Comparison of V4-TMR binding to LPS, lipid A and PC

Upon addition of V4-TMR to LPS, lipid A, and PC, the ACF changed significantly with the different binding processes. Fig. 5 shows the autocorrelation function of 100 nM V4-TMR mixed with 10 μM LPS, lipid A or PC. A concentration of 10 μM was chosen since at this level binding of V4-TMR to LPS was saturated as shown in the previous experiment. The detailed data are given in Table 2. The mixture of V4-TMR with PC showed similar ACFs and photon count rates as V4-TMR. Assuming again the first particle to be an impurity of free TMR, a two-particle model was used for data fitting. The second particle exhibited an F_2 of 4.2% and an increase in the fluorescence yield compared to TMR of Q_2/Q_1 of 3.21.

Table 1
Comparison of TMR, V4-TMR, V4-TMR: LPS on coverslip

	Intensity on surface [AU]	Intensity in solution [AU]
PBS	1.37±9.50	0.40±0.02
100 nM TMR	3432±682	423±5
5 μM V4-TMR	306±220	23±2
5 μM V4-TMR: 50 μM LPS	1511±455	727±3

However, the V4-TMR: LPS and V4-TMR: lipid A mixtures showed stronger changes in the ACFs. The apparent number of particles in these solutions increased to 0.324 for LPS and 0.095 for lipid A. Concomitantly, an increase in the overall photon count rates was observed, yielding 30.8 kHz and 11.2 kHz for the LPS and lipid A solutions, respectively. The fluorescence yield of the V4-TMR: LPS and V4-TMR: lipid A complexes compared to TMR was $Q_2/Q_1 \approx 2$. Both, V4-TMR: LPS, V4-TMR: lipid A had a τ_D of 1 to 2 ms. The molar fraction of complexes in solution, F_2, were 80.8% and 43.5% for V4-TMR: LPS and V4-TMR: lipid A, respectively.

3.7. Binding of V4-TMR to SUVs of pure lipids

The interaction of V4-TMR (200 nM) with POPG, POPC, POPE, DPPG, DPPC and DPPE was compared by studying mixtures of V4-TMR with SUVs in PBS. The concentration of lipids was in all cases 50 μM. A two-particle model was used for data fitting, with the first diffusion time τ_{D1} fixed to 52 μs. The values for the second particle, τ_{D2}, F_2 and N_2 are shown in Fig. 6. The diffusion time of the larger particle τ_{D2} was in all cases between 0.6 and 1.7 ms, similar to the expected diffusion time of lipid SUVs. However, F_2 and N_2 differed markedly depending on the lipid used. In the group of lipids with unsaturated lipid tails, the highest values for these parameters

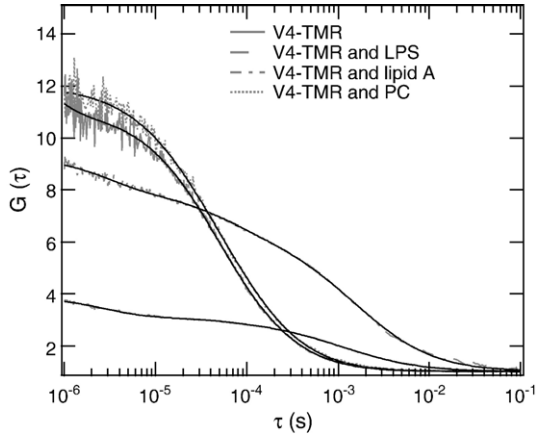

Fig. 5. Comparison of autocorrelation functions of V4-TMR and the complexes of V4-TMR with LPS, lipid A and PC. The concentration of V4-TMR was 100 nM; the concentrations of LPS, lipid A and PC were 10 μM. Fits to the data are given in solid lines.

Table 2
Comparison of interaction of V4-TMR peptide with LPS, lipid A and PC

	C (kHz)[a]	N_{app}	τ_{D1} [μs]	τ_{D2} [ms]	F_2 [%]	Q_2/Q_1[b]	N_2
V4-TMR	3.8±0.3	0.064±0.004	52.5±1.8	–	–	–	–
V4-TMR:LPS	30.8±0.7	0.324±0.005	52.5[c]	1.08±0.07	80.8±0.2	1.73±0.28	0.270±0.004
V4-TMR:lipid A	11.2±1.3	0.095±0.009	52.5[c]	1.89±0.17	43.5±4.3	2.52±0.28	0.050±0.009
V4-TMR:PC	4.3±0.2	0.058±0.002	52.5[c]	1.87±2.59	4.2±1.2	3.21±0.37	0.003±0.001

[a] C is the overall count rate.
[b] Q_1 is 59.5 kHz for free TMR.
[c] τ_{D1} was fixed in data fitting.

were obtained for POPG. In the group with saturated lipid tails the differences were smaller but DPPG still showed the highest F_2 and N_2.

3.8. Interaction of V4-TMR with mixed lipid SUVs

Gram-negative bacteria have a unique outer membrane, which is negatively charged. Because of the similar net negative charge of POPG, it is widely used to mimic the bacterial outer membrane to study the interaction with antimicrobial peptides. We thus used the mixture of POPE/POPG=2/1 to mimic the bacterial outer membrane compared to mixtures of POPC/POPE=3/1 mimicking mammalian membranes (Fig. 7). In solutions of 200 nM V4-TMR and 50 μM of these lipid mixtures, the POPE/POPG SUVs showed a similar ACF with that of pure POPG SUVs. The value of F_2 and N_2 were both very close to those of pure POPG SUVs, although the mole fraction of POPG in the mixture lipid was only 33%. However, POPC/POPE SUVs had smaller values of F_2 and N_2 compared to POPG SUVs. The diffusion time of V4-TMR: mixed lipids SUVs complex was similar to that of pure lipids SUVs, between 0.6 and 1 ms.

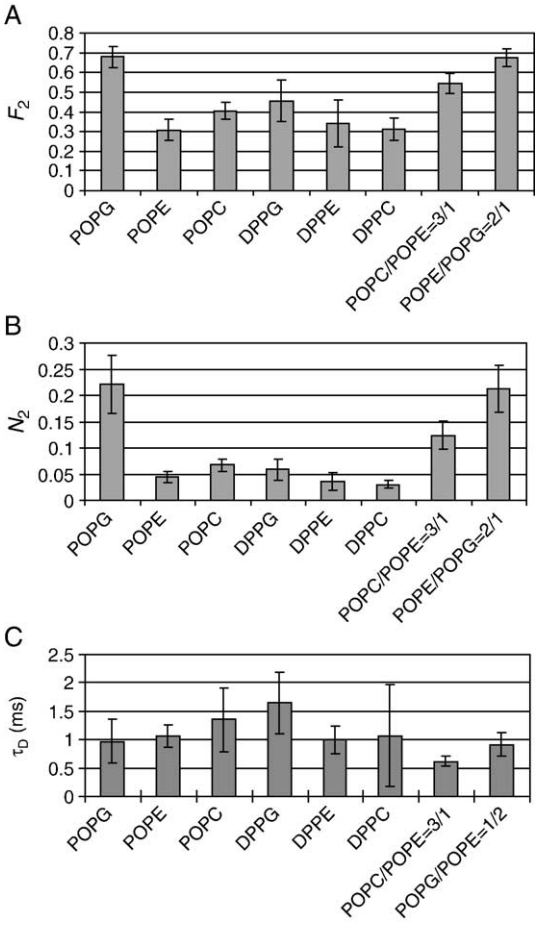

Fig. 6. Comparison of V4-TMR binding to different SUVs. (A) F_2 and (B) N_2 indicate different binding affinity when V4-TMR binds to different lipid SUVs. (C) Comparison of the diffusion time of SUVs bound by V4-TMR. All data were fitted with a two-particle model. The diffusion time of the fast diffusing particle (impurities of free TMR) was between 52 and 67 μs. The slowly diffusing particle (V4-TMR bound to SUVs) fell mostly in a range from 0.9 to 1.5 ms, as expected for the SUVs. The concentration of V4-TMR was 200 nM. The total lipid concentration was 50 μM.

3.9. Interaction of V4 with fluorophore entrapped LUVs

LUVs composed of POPG were used to investigate the interaction of V4 with vesicles at a high peptide/lipid ratio. Fig. 8 depicts the process of the leakage of fluorophore entrapped LUVs (20 μM POPG lipid concentration) caused by V4 (10 μM). The leakage occurred in less than 10 min. At the beginning, the Rho 6G entrapped LUVs diffused as large fluorescent particles, whose diffusion time was 6.46±2.56 ms (Fig. 8A). After less than 4-min incubation with V4 two diffusion times could be detected. The two fluorescent species in the solution have diffusion times of 47.2±4.2 μs and 24.6±8.7 ms (Fig. 8B). After 8 min, there

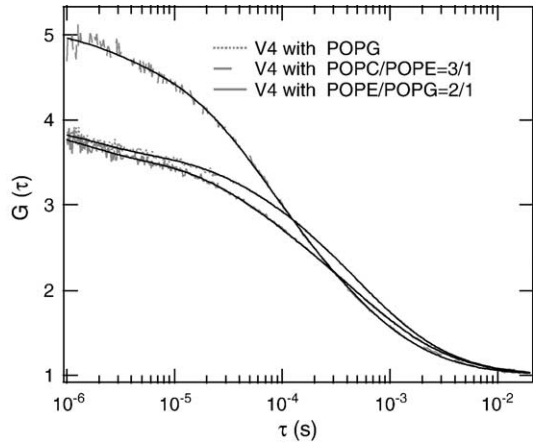

Fig. 7. Binding of V4-TMR to SUVs of mixed lipid composition. Shown are autocorrelation functions of V4-TMR bound to SUVs made of either POPG or mixtures of POPC/POPE (3:1) or POPE/POPG (2:1). The concentration of V4-TMR was 200 nM. The total lipid concentration was 50 μM. Fits to the data are shown in solid lines.

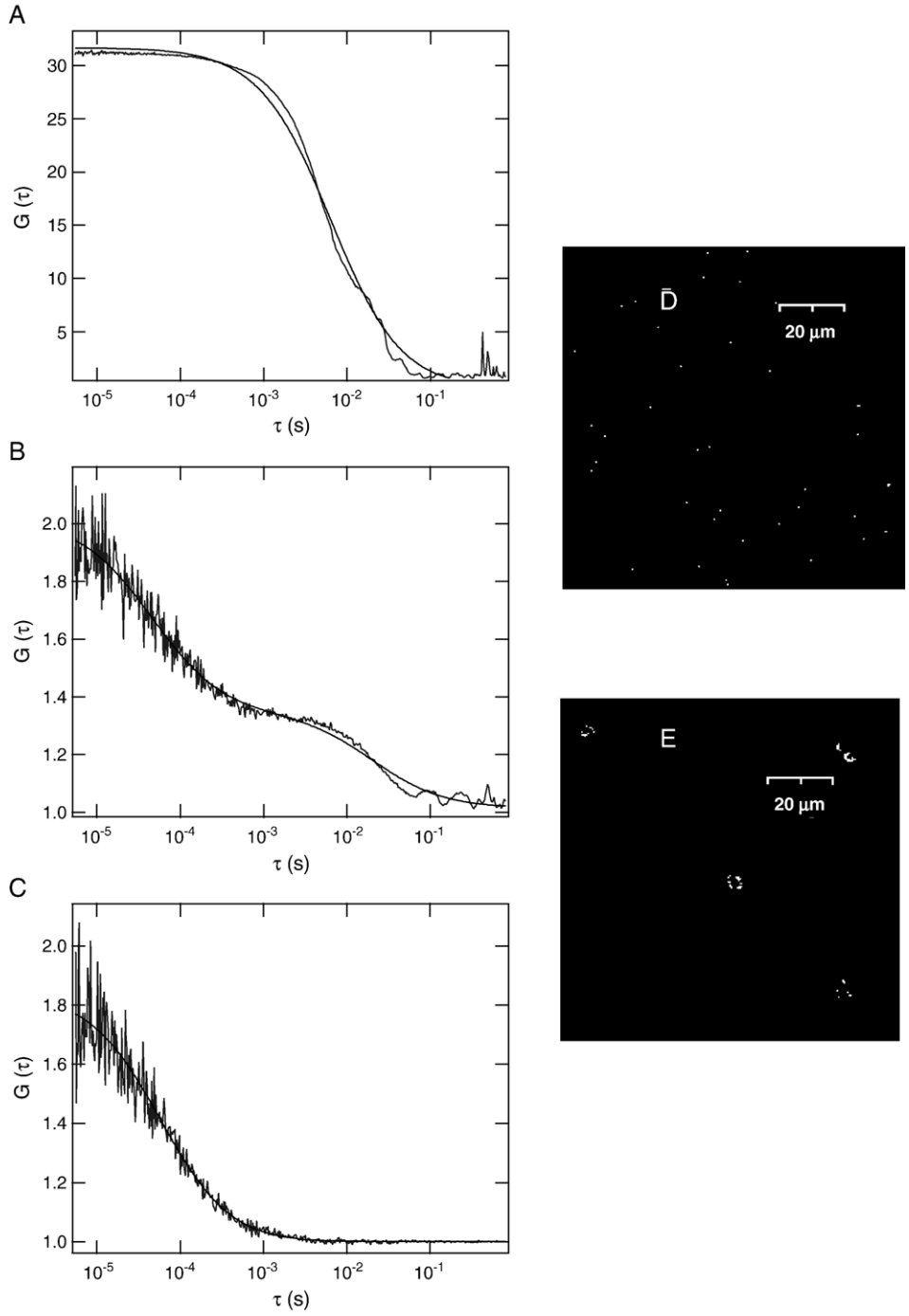

Fig. 8. Leakage of fluorophore entrapped LUVs (20 μM POPG lipid) was caused by V4 (10 μM) in less than 10 min. (A) At the beginning LUVs with Rho 6G entrapped diffused as large fluorescent particle with a diffusion time on the order of 6 ms. (B) After less than 4 min, leakage occurred with some Rho 6G released into the solution from vesicles. The free Rho 6G was detected as a particle with a diffusion time of 47.2±4.2 μs. In addition, some large-size particles appeared in the solution with long diffusion time of more than 20 ms. (C) After 8 min, only released Rho 6G can be detected with the diffusion time of 54.7±4.8 μs. (D) Confocal image of fluorophore labeled LUVs without peptide. (E) Confocal image of fluorophore labeled LUVs with peptide after 5 min.

was only one fluorescent species detected in the solution with a diffusion time of 54.7±4.8 μs (Fig. 8C). This value compared well with the diffusion time of Rho 6G of 56.6±1.3 μs, which indicated that the Rho 6G entrapped inside the LUVs has been released into solution. Controls with LUVs made of POPC (lipid concentration 20 μM) did not show any obvious leakage up to a concentration of 10 μM V4.

3.10. Interaction of V4 with fluorophore labeled LUVs

Initially 20 μM fluorophore labeled LUVs (lipid concentration) and 10 μM V4 were mixed. This led to a strong decrease in photon count rates and large aggregates occasionally appeared in the solution. We thus used confocal microscopy to determine the fate of the vesicles. Without peptide, the fluorophore labeled LUVs in solution were below the

resolution limit due to their size of about 100 nm (Fig. 8D) and were seen as single spots. However, upon the addition of V4 into the solution followed by incubation of 5 min, obvious large fluorescent aggregates appeared (Fig. 8E) with less particles in solution.

4. Discussion

4.1. V4-TMR aggregates and is strongly quenched in PBS

V4-TMR solutions at 100 nM exhibit very low fluorescence and ACFs with unexpectedly low number of particles and very short diffusion times. A comparison of the ACF of 100 nM V4-TMR with 1 nM TMR solution showed that the diffusion time and fluorescence yield Q in the two solutions were similar. The number of particles in the confocal volume for the V4-TMR solution was 5 times lower than for free TMR despite its 100 times higher concentration. We thus suggest that the fluorescent particles seen in these solutions are actually free TMR and the peptide itself is quenched and cannot be detected, except for rare isolated peaks. Comparing the numbers of particles detected in the two solutions, the proposed impurity of free TMR in V4-TMR solution would be 0.18%, which is well within the limits of the manufacturer. The intensity of V4-TMR on the coverslip surface and in solution from confocal imaging confirmed the result (Table 1). The fluorescence intensity of 5 μM V4-TMR is much lower than that of 100 nM TMR both on coverslip and in solution. Assuming that there is 0.18% impurity of TMR in the V4-TMR solution, a concentration of 9 nM free TMR will be expected. Thus the 100 nM TMR solution has a $100/9 \approx 11$ times higher TMR concentration. Comparing the surface fluorescence of the 100 nM TMR to the 5 μM V4-TMR shows that the surface peak is about $3432/306 \approx 11$ times higher, which implies that most fluorescence seen on the surface stems from free TMR.

The rare occurrence of large count rate peaks in the solution together with the results from titrating V4 with R18, where large, slow diffusing fluorescent peaks were seen, point towards peptide aggregation. The aggregation is a consequence of the strong hydrophobicity of the peptide and leads to self-quenching of the fluorophores. However, the multiple positive charges on the peptide should act against aggregation. To test this hypothesis, we made FCS measurements of V4-TMR in de-ionized water. In contrast to PBS the lack of ions which shield electrostatic interactions should lead to a decrease in aggregation and of self-quenching. This was found to be the case and in pure water the measured number of particles of V4-TMR in the confocal volume rose and a larger number of smaller aggregates were seen. However, the peptide was still not completely dissolved. Similarly, attempts to dissolve the peptide in the detergent Triton-X100 or DMSO failed. Therefore, we suggest that the peptide in PBS is strongly quenched due to aggregation and only free TMR impurities can be detected in FCS.

This opens the possibility that quenched aggregated V4-TMR attached to the coverslip and escaped detection in the confocal studies. However, the confocal study in the presence of LPS shows that even if aggregated V4-TMR should have attached to the coverslip, only a small part of this attached V4-TMR can be activated and the increase of the fluorescence, as expected during V4-TMR: LPS binding (Table 2), is on the same order of magnitude as the fluorescence increase in solution (Table 1).

4.2. LPS and lipids can partly dissolve V4

When V4-TMR at constant concentration was titrated with increasing concentration of LPS or lipids, the photon count rates of the mixture and the apparent number of particles detected both increased (Figs. 4 and 5). It should be noted that the increases were strongest for lipids which are supposed to have a high affinity for V4 based on their negative charge. Hence, LPS and POPG showed strong increases due to the putative electrostatic interactions while the other lipids and lipid mixtures showed smaller changes. This can be explained by two effects: (i) The interaction of V4-TMR with LPS or lipids leads to a disaggregation of V4-TMR aggregates which previously existed due to the strong hydrophobicity of the peptide and in which TMR is strongly quenched; in other words, the V4-TMR peptide was solubilised by LPS or lipids. The disaggregation thus leads to an increase in fluorescence as well as an apparent increase in the number of particles observed. It should be noted however, that none of the lipids can dissolve the peptide completely. A comparison of N detected in the case of saturated binding (100 nM V4, 10 μM LPS, $N_2 = N \times F_2 = 0.270$) with a 1 nM TMR solution ($N = 0.349$) indicates that less than 0.77% of the peptide is dissolved. ii) TMR, the fluorescent label attached to V4, comes into a different local environment upon binding (local pH, polarity) leading to an increase in its fluorescence yield Q. Both effects will lead to an increase in the number of particles N and an increase in photon count rates as observed. From the data we have estimated Q for the V4-TMR: LPS and V4-TMR: lipid A complex in its hydrophobic environment to be about twice as bright as free TMR in aqueous solution (Table 2). This change in fluorescence yield is an effect of the local environment of the fluorophore and cannot be attributed to multiple peptides binding to one vesicle or micelle since at the low concentrations of V4-TMR used compared to the lipid concentrations, it is unlikely to find more than one peptide bound per lipid complex.

Experiments with FITC-LPS support this hypothesis of peptide disaggregation. In these measurements no changes in diffusion time or the number of particles could be detected, indicating that (i) V4 does not disaggregate LPS micelles as has been shown for other antimicrobial peptides [38], and (ii) none of the large V4 aggregates detected in the titration experiment with R18 are binding to LPS. This indicates that the peptide is actually disaggregated when binding to LPS or lipids.

Therefore, to increase the fraction of peptide that is active, the peptide should be redesigned by embedding the binding pattern in a more hydrophilic or amphipathic structure to increase the solubility and facilitate the disaggregation of the peptide by LPS and bacterial membrane-like lipids.

4.3. V4-TMR functions via hydrophobic and electrostatic forces

It has been suggested that electrostatic and hydrophobic interactions are predominant forces driving the binding process between antimicrobial peptides and membranes [20]. V4 is a very hydrophobic peptide with 8 valines among 19 residues. The high hydrophobicity gives the peptide a tendency to self-aggregate and to interact with alkyl chains of LPS and other lipids. Besides its predominant hydrophobic nature, its highly positive charge with 4 lysines helps in interacting with the phosphate groups of the lipid A moiety of LPS and lipids with negative charge, such as POPG and DPPG. The importance of electrostatic interactions in comparison to hydrophobic interactions can be seen from the experiments. Despite having the same lipid tail groups the affinity of V4-TMR was higher for POPG, an anionic lipid, than for POPC and POPE, both zwitterionic lipids. This indicates that electrostatic interaction is the major driving force for the binding process. DPPG, DPPE and DPPC also showed the same results in pure lipid SUVs. In the mixed lipids POPG/POPE, although the fraction of POPG was only 33%, the binding efficiency was almost the same as that of pure POPG. The strong binding of V4-TMR to negative lipids vesicles was the reason for the selectivity of the peptide for bacterial membranes in contrast to mammalian membranes. The structural integrity of the LPS molecules was significant in the binding process. The results showed that the full, intact LPS molecule is needed for maximal binding affinity. The binding efficiency of V4-TMR with lipid A was lower than that of LPS despite the fact that lipid A is considered to be the bioactive part of LPS.

4.4. Saturation of lipids affects the binding with V4-TMR

The affinity of V4-TMR for lipids SUVs with the same head group was always larger for unsaturated lipids (POPG, POPE, POPC) than for saturated lipids (DPPG, DPPE, DPPC) as shown in Fig. 6B. The double bond of the unsaturated lipids increases the fluidity of the lipid bilayer, leading to less dense packing of the unsaturated lipid molecules. This provides V4-TMR better access to the unsaturated lipid molecules and increases the chance of insertion into the bilayer. In addition, the interaction between V4-TMR and the lipid tail groups is facilitated for the unsaturated lipids due to the larger flexibility of the tail groups [39]. Both effects, the packing of lipid molecule in the bilayer, and the flexibility of the tail groups, could contribute to the higher binding affinity of V4-TMR for unsaturated lipids.

4.5. The mechanism of interaction between V4 and lipid vesicles

Although V4 can bind LPS, lipid A and other artificial lipids at a very low peptide/lipid ratio, the leakage of vesicles in the presence of V4 can only be observed at a higher peptide/lipid ratio. Considering that the large peptide aggregates are not active and only about 0.77% of the peptide is active, leakage was observed at a peptide/lipid ratio of 1:260. The diameter of LUVs is around 100 nm and the area of each lipid molecule is 0.4 nm^2 [41], therefore the ratio of peptide to LUVs is estimated to be 606:1. When the concentration of peptide decreased to a ratio of 1:2600 (peptide/LUVs=61:1), there was no observable leakage. Compared to V4-TMR binding to different lipid SUVs, the peptide/SUVs is about 1.2:1 which is much lower and more peptide is needed to make the vesicles permeable. Confocal imaging showed that POPG LUVs fused within 5 min. Since these large aggregates were relatively few in number, they were observed in only some of the FCS measurements if at all. The results from confocal imaging were consistent with the interpretation of leakage and fusion of vesicles. V4 might first bind to the surface of the vesicles through electrostatic interactions with the hydrophilic headgroup of the lipids. Conformational changes of the peptide could then cause the hydrophobic part of the peptide to interact with the alkyl chains of the lipids by a strengthened hydrophobic interaction. When a threshold concentration of V4 is reached, the lipid membrane is disrupted and becomes permeable. At the same time V4, which has two hydrophobic arms, might act as a linker between vesicle fragments and thus lead to lipid vesicles aggregation forming the large particles shown in Fig. 8D and E.

5. Conclusion

Antimicrobial peptides have elicited great interest due to their potential clinical use. In this paper we applied fluorescence correlation spectroscopy to investigate the action of a rationally designed antimicrobial peptide V4. We have shown for the first time, to our knowledge, that a simple amphipathic cationic pattern BHBHB in a cyclized structure is sufficient to impart selectivity and antimicrobial activity. V4 was shown to bind selectively to negatively charged lipids, typically found in bacteria. At a peptide/lipid ratio of 1:260 (peptide/LUVs=606:1) this peptide can render large unilamellar vesicles permeable and cause vesicle fusion. Considering that only less than 1% of the peptide is active, the antimicrobial activity is expected to increase greatly if the peptide solubility can be increased. Therefore it is necessary to design a peptide containing the identified binding patterns but in a more hydrophilic or detergent-like structure which would increases solubility and possibly the activity of the peptide.

Acknowledgements

The research in this work was funded by a grant from the faculty research committee of the NUS. LY acknowledges support by a NUS graduate scholarship.

References

[1] R.A. Bonomo, Multiple antibiotic-resistant bacteria in long-term-care facilities: an emerging problem in the practice of infectious diseases, Clin. Infect. Dis. 31 (2000) 1414–1422.
[2] M. Stark, L.P. Liu, C.M. Deber, Cationic hydrophobic peptides with antimicrobial activity, Antimicrob. Agents. Chemother. 46 (2002) 3585–3590.

[3] J.D. Williams, Antibiotic resistance in hospital pathogens—Acquisition or spread? Int. J. Antimicrob. Agents 18 (2001) 295–298.
[4] M. Zasloff, Magainins, a class of antimicrobial peptides from *Xenopus* skin: isolation, characterization of two active forms, and partial cDNA sequence of a precursor, Proc. Natl. Acad. Sci. U. S. A. 84 (1987) 5449–5453.
[5] D. Barra, M. Simmaco, Amphibian skin: a promising resource for antimicrobial peptides, Trends Biotechnol. 13 (1995) 205–209.
[6] A. Tossi, L. Sandri, A. Giangaspero, Amphipathic, α-helical antimicrobial peptides, Biopolymers (Peptide Science) 55 (2000) 4–30.
[7] T. Ganz, R.I. Lehrer, Antimicrobial peptides of vertebrates, Curr. Opin. Immunol. 10 (1998) 41–44.
[8] Y. Jin, H. Mozsolits, J. Hammer, E. Zmuda, F. Zhu, Y. Zhang, M.I. Aguilar, J. Blazyk, Influence of tryptophan on lipid binding of linear amphipathic cationic antimicrobial peptides, Biochemistry 42 (2003) 9395–9405.
[9] H. Steiner, D. Hultmark, Å. Engström, H. Bennich, H.G. Boman, Sequence and specificity of two antibacterial proteins involved in insect immunity, Nature 292 (1981) 246–268.
[10] M.E. Selsted, S.S. Harwig, T. Ganz, J.W. Schilling, R.I. Lehrer, Primary structure of three human neutrophil defensins, J. Clin. Invest. 76 (1985) 1436–1439.
[11] R.I. Lehrer, A.K. Lichtenstein, T. Ganz, Defensins: antimicrobial and cytotoxic peptides of mammalian cells, Annu. Rev. Immunol. 11 (1993) 105–128.
[12] Y. Sokolov, T. Mirzabekov, D.W. Martin, R.I. Lehrer, B.L. Kagan, Membrane channel formation by antimicrobial protegrins, Biochim. Biophys. Acta 1420 (1999) 23–29.
[13] W.T. Heller, A.J. Waring, R.I. Lehrer, H.W. Huang, Multiple states of β-sheet peptide protegrin in lipid bilayers, Biochemistry 37 (1998) 17331–17338.
[14] C. Lawyer, S. Pai, M. Watabe, P. Borgia, T. Mashimo, L. Eagleton, K. Watabe, Antimicrobial activity of a 13 amino acid tryptophan-rich peptide derived from a putative porcine precursor protein of a novel family of antibacterial peptides, FEBS Lett. 390 (1996) 95–98.
[15] M.E. Selsted, M.J. Novotny, W.L. Morris, Y.Q. Tang, W. Smith, J.S. Cullor, Indolicidin, a novel bactericidal tridecapeptide amide from neutrophils, J. Biol. Chem. 267 (1992) 4292–4295.
[16] E.J. Helmerhorst, P. Breeuwer, W. van't Hof, E. Walgreen-Weterings, L.C. Oomen, E.C. Veerman, A.V. Amerongen, T. Abee, The cellular target of histatin 5 on *Candida albicans* is the energized mitochondrion, J. Biol. Chem. 274 (1999) 7286–7291.
[17] R.M. Epand, H.J. Vogel, Diversity of antimicrobial peptides and their mechanisms of action, Biochim. Biophys. Acta 1462 (1999) 11–28.
[18] V. Frecer, B. Ho, J.L. Ding, Interpretation of biological activity data of bacterial endotoxins by simple molecular models of mechanism of action, Eur. J. Biochem. 267 (2000) 837–852.
[19] N. Sitaram, R. Nagaraj, Interaction of antimicrobial peptides with biological and model membranes: structural and charge requirements for activity, Biochim. Biophys. Acta 1462 (1999) 29–54.
[20] V. Frecer, B. Ho, J.L. Ding, De novo design of potent antimicrobial peptides, Antimicrob. Agents Chemother. 48 (2004) 3349–3357.
[21] D. Magde, E. Elson, W.W. Webb, Thermodynamic fluctuations in a reacting system—Measurement by fluorescence correlation spectroscopy, Phys. Rev. Lett. 29 (1972) 705–708.
[22] N.L. Thompson, in: J.R. Lakowicz (Ed.), Topics in Fluorescence Spectroscopy, Plenum Press, New York, 1991, pp. 337–378.
[23] S. Maiti, U. Haupts, W.W. Webb, Fluorescence correlation spectroscopy: diagnostics for sparse molecules, Proc. Natl. Acad. Sci. U. S. A. 94 (1997) 11753–11757.
[24] J. Widergren, R. Rigler, Fluorescence correlation spectroscopy as a tool to investigate chemical reactions in solutions and on cell surfaces, Cell. Mol. Biol. 44 (5) (1998) 857–879.
[25] W.W. Webb, Fluorescence correlation spectroscopy: inception, biophysical experimentations, and prospectus, Appl. Opt. 40 (2001) 3969–3983.
[26] O. Krichevsky, G.. Bonnet, Fluorescence correlation spectroscopy: the technique and its applications, Rep. Prog. Phys. 65 (2) (2002) 251–297.
[27] A. Pramanik, P. Thyberg, R. Rigler, Molecular interactions of peptides with phospholipid vesicle membranes as studied by fluorescence correlation spectroscopy, Chem. Phys. Lipids 104 (2000) 35–47.
[28] L. Rusu, A. Gambhir, S. McLaughlin, J. Rädler, Fluorescence correlation spectroscopy studies of peptide and protein binding to phospholipid vesicles, Biophys. J. 87 (2004) 1044–1053.
[29] E.L. Elson, D. Magde, Fluorescence correlation spectroscopy. I. Conceptual basis and theory, Biopolymers 13 (1974) 1–27.
[30] M. Ehrenberg, R. Rigler, Rotational Brownian motion and fluorescence intensity fluctuations, Chem. Phys. 4 (1974) 390–401.
[31] P. Kask, R. Günther, P. Axhausen, Statistical accuracy in fluorescence fluctuation experiments, Eur. Biophys. J. 25 (1997) 163–169.
[32] T. Wohland, R. Rigler, H. Vogel, The standard deviation in fluorescence correlation spectroscopy, Biophys. J. 80 (2001) 2987–2999.
[33] S.R. Aragon, R. Pecora, Fluorescence correlation spectroscopy as a probe of molecular dynamics, J. Chem. Phys. 64 (1976) 1791–1803.
[34] U. Meseth, T. Wohland, R. Rigler, H. Vogel, Resolution of fluorescence correlation spectroscopy, Biophys. J. 76 (1999) 1619–1631.
[35] D.E. Koppel, Statistical accuracy in fluorescence correlation spectroscopy, Phys. Rev., A 10 (1974) 1938–1945.
[36] S.T. Hess, W.W. Webb, Focal volume optics and experimental artifacts in confocal fluorescence correlation spectroscopy, Biophys. J. 83 (2002) 2300–2317.
[37] N.S. Tan, B. Ho, J.L. Ding, High-affinity LPS binding domain(s) in recombinant factor C of a horseshoe crab neutralizes LPS-induced lethality, FASEB 14 (2000) 859–870.
[38] P. Li, T. Wohland, B. Ho, J.L. Ding, Perturbation of lipopolysaccharide (LPS) micelles by sushi 3 (S3) antimicrobial peptide, J. Biol. Chem. 279 (2004) 50150–50156.
[39] D. Gidalevitz, Y. Ishitsuka, A.S. Muresan, O. Konovalov, A.J. Waring, R.I. Lehrer, K.Y.C. Lee, Interaction of antimicrobial peptide protegrin with biomembrane, Proc. Natl. Acad. Sci. U. S. A. 100 (2003) 6302–6307.
[40] J. Widengren, R. Rigler, U. Mets, Triplet-state monitoring by fluorescence correlation spectroscopy, J. Fluoresc. 4 (1994) 255–258.
[41] B. Alberts, A. Johnson, J. Lewis, M. Raff, K. Roberts, P. Walter, Molecular Biology of the Cell, 4th ed., Garland Publishing, Inc., New York, 2002, p. 584.